Experimental Investigation of Circumferentially Non-Uniform Heat Flux on the Heat Transfer Coefficient in a Smooth Horizontal Tube with Buoyancy Driven Secondary Flow

J. Dirker*, J.P. Meyer and W.J. Reid

Department of Mechanical and Aeronautical Engineering, University of Pretoria, Pretoria, Private Bag X20, Hatfield 0028, South Africa.

*Corresponding Author:

Email Address: jaco.dirker@up.ac.za

Phone: +27 (0)12 420 2465

Fax: +27 123625124

Highlights

- Experimental investigation of mixed convection for non-uniform heating.
- Heat flux intensity, heating span and heating positions are investigated.
- Heating position effects are significant and are characterised.
- New Nusselt number correlations are presented.

Abstract

In this experimental investigation the influence of non-uniform heat flux distributions on the internal heat transfer coefficient in a horizontal circular tube was studied for liquid water. The tube had an inner diameter of 27.8 mm and a length to diameter ratio of 72. Different outer wall heat flux conditions were studied for Reynolds numbers ranging from 650 to 2600 at a Prandtl number of approximately 6.5. Heat flux distributions included fully uniform heating (which had a circumferential angle span of 360°) and different partial uniform heat flux distributions with angle spans of 180° or 90° at different circumferential positions. Depending on the angle span, local heat flux intensities ranging from 1658 W/m^2 to 6631 W/m^2 were tested. Results indicated that the average steady state Nusselt number is greatly influenced by the applied heat flux position and intensity. Highest average heat transfer coefficients were achieved for cases where the applied heat flux was positioned on the lower half (in terms of gravity) of the tube circumference, while the lowest heat transfer coefficients were achieved when the heating was applied to the upper half of the tube. Smaller angle spans produced lower heat transfer coefficients. The relative thermal performance of the different heating scenarios where characterised and described by means of newly developed heat transfer coefficient correlations for angle spans of 180° and 90° which correlated 95% and 96% of the data respectively within 3% of the measured Nusselt number.

Keywords: Non-uniform heat flux, Nusselt number, Richardson number, mixed convection.

Nomenclature

A	Area [m²]
C	Correlation coefficient [-]
c_p	Specific heat [J/kgK]
D, D_0	Diameter and outer diameter [m]
EB	Energy balance error [%]
g	Gravity [m/s²]
Gr	Grashof number [-]
h	Heat transfer coefficient [W/m^{2}K]
h^*	Hypothetically assumed heat transfer coefficient [W/m^{2}K]
$\bar{h}$	Average heat transfer coefficient [W/m^{2}K]
I	Electric current [A]
j	Colburn j-factor [-]
k	Thermal conductivity [W/mK]
L	Length [m]
M	Correlation exponent [-]
m	Measuring station index number [-]
$\dot{m}$	Mass flow rate [kg/s]
N	Correlation exponent [-]
n	Thermocouple position
$\mathrm{Nu}, \overline{\mathrm{Nu}}$	Nusselt number and average Nusselt number [-]
P	Correlation exponent [-]
Pr	Prandtl number [-]
$\dot{Q}$	Heat transfer rate [W]
$\dot{q}$	Heat flux [W/m^2]
$r, \bar{r}$	Radial position and average radial position [m]
r_1	Inner radius of Insulation [m]
r_2	Outer radius of insulation [m]
R	Thermal resistance [K/W]
Re	Reynolds number [-]
Ri	Richardson number [-]
$T, \bar{T}$	Temperature and average temperature [˚C]
t	Wall thickness [m]
V	Voltage [V] or velocity [m/s]

Greek symbols

β	Coefficient of thermal expansion [-]
ρ	Density [kg/m^3]
μ	Dynamic viscosity [kg/ms]
ν	Kinematic viscosity [m²/s]
φ	Characteristic angular position of heated span [°]

Subscripts

amb	Ambient
B	Bulk
ci	Calculated value
DC	Direct Current
h	Heated
i	Inner
in	Inlet / Input
$insul$	Insulation
$LMTD$	Logarithmic mean temperature difference
$loss$	Heat loss
m	Measuring station position number
mid	midpoint
n	Circumferential thermocouple position number
out	Outlet / Output
s	Surface
TC	Thermocouple
tot	Total
w	Wall
water	Water

1. Introduction

Several applications including, but not limited to, solar collectors and boiler systems contain circular tubes that are exposed to circumferential non-uniform heat flux or wall temperature thermal boundaries. However, relatively little research has been performed to investigate the characteristics of circumferential non-uniform thermal conditions in terms of the effective convective heat transfer coefficient. This has led to significant uncertainty regarding the convective heat transfer ability of circular flow passages, especially for conditions where buoyancy driven secondary flow is present.

Such conditions, known as mixed convection are specifically prevalent at low Reynolds numbers if the thermal boundary condition significantly impacts the fluid density distribution within the passage. In these cases, both the influence of the mechanically forced flow component, as well as the natural convection component must be considered.

Mixed convection can result in enhanced heat transfer or suppressed heat transfer depending on the directional components of the forced and buoyancy flow terms. In this sense the thermal boundary is very important and can be described either in terms of temperature (uniform or non-uniform), in terms of heat flux (uniform or non-uniform), or in terms of both temperature and heat flux.

Several studies have been conducted for uniform heat flux conditions. Yasuo *et al.* [1] experimentally investigated the buoyancy effects on air flowing in a horizontal tube under uniform heat flux conditions for a Reynolds number range of 100 to 13 000. They showed that the local Nusselt number is significantly influenced when the product of the Reynolds and Rayleigh numbers is higher than 1000. Kupper *et al.* [2] experimentally investigated mixed convection in a circular horizontal tube for Reynolds numbers ranging from 100 to 2000 and Grashof numbers ranging from 300 to 30 000. They showed that an increase in the Grashof or Reynolds numbers resulted in higher Nusselt numbers and that an entry length is needed in order to establish secondary flow. Bergles and Simonds [3] experimentally investigated the effects of mixed convection for a Reynolds number range of 460 to 720. They found that the Nusselt number can be greatly affected by the presence of secondary flow and that the heat transfer coefficient can be up to three or four times higher compared to predictions of traditional correlations for pure forced convection. Morcos and Bergles [4] continued the experimental investigation for distilled water and ethylene glycol. Their data indicated that the Nusselt number is influenced by the Rayleigh number, variations of the thermo-physical properties of the heat transfer fluid, and the radial conduction in the tubes wall. They proposed a Nusselt number correlation which can be used for a wide variety of fluid properties and flow conditions. Chou and Hwang [5] carried out a numerical analysis of the Graetz problem with the presence of natural convection for uniform heat flux. They used the vorticity-velocity method and coupled it to the Boussinesq

approximation to model the temperature dependence of the fluid density. They showed that natural convection distorts the axial flow velocity and cross-sectional temperature profiles and that the highest fluid velocity and lowest fluid temperature can be found at the bottom of the tube. Ghajar and Tam [6] experimentally considered water and ethylene glycol as the working fluid in a horizontal circular tube for a large range of Reynolds numbers covering the laminar flow regime to the turbulent flow regime. They also showed the need for an entrance length in order to allow the development of the secondary flow. They proposed a Nusselt number correlation for the laminar flow regime in terms of the Reynolds number, Prandtl number, the length to diameter ratio, the Grashof number and a wall viscosity ratio. Mohammed and Salman [7] experimentally investigated mixed convection in developing flow for air in circular tubes with a uniform heat flux for a Reynolds number range of 400 to 1 600. They found that secondary flow could have different effects on the Nusselt number depending on the Reynolds number. The Nusselt number decreased at lower Reynolds numbers and increased at higher Reynolds numbers, or when higher heat flux was applied. They correlated the average Nusselt number as a function of the Rayleigh and Richardson numbers.

Some work has also been done on flow passages with non-uniform heating. Lin and Lin [8] experimentally investigated the effect of non-uniform (bottom) heating on air flow in a horizontal rectangular duct for Reynolds numbers ranging from 9 to 186. They included flow visualization of the secondary flow vortices and showed that the onset of thermal instability, which enhances the heat transfer, occurs close to the duct entrance with increased Grashof numbers and decreased Reynolds numbers. Elatar and Siddiqui [9] experimentally investigated water flow in a horizontal square duct with bottom heating for Reynolds numbers ranging from 300 to 750 and Grashof numbers ranging from 6.37×10^6 to 3.86×10^7. They showed that the effect of secondary flow was dependent on the Reynolds and Grashof numbers and that turbulence intensity is increased due to rising plumes of warm fluid. Back flow along the top unheated wall, which increased in intensity with the lower wall temperature, was observed at higher Richardson numbers. Chang *et al.* [10] experimentally and numerically considered upper hemispherical heating of horizontal circular tubes for water under forced convection in the turbulent flow regime. They found that the well-known Dittus-Boelter correlation correctly predicted the average Nusselt number irrespective of heat flux distribution as can be expected from the absence of mixed convection. Okafor *et al.* [11, 12] included mixed convection in their numerical investigation of circumferential non-uniform heating of a horizontal circular tube with water as working fluid. They considered a sinusoidal type heat flux distribution for a length to diameter ratio of 159 and a Reynolds number range of 180 to 2 200 and used the Boussinesq approximation to model the temperature dependence of the fluid density. It was found that the Nusselt number (average and local) are enhanced due to the presence of non-uniform heating

occurring from below. Huang et al.[13] also performed a numerical study on the effects of non-uniform heat flux boundary conditions for fully developed flow in a circular tube. They considered upper and lower heating as well as fully uniform heating for flow in the turbulent regime for super-heated steam. When comparing uniform heat flux cases and non-uniform heat flux cases they observed a marked difference between the velocity fields, temperature distribution, flow resistance and heat transfer. They also noted that the Nusselt number is larger for the non-uniform heat flux cases.

Of interest due to its impact on buoyancy driven secondary flow, it is also important to note that work has also been done on uniform wall temperature boundary conditions. For instance, Oliver [14] experimentally investigated the effect of natural convection on the heat transfer in horizontal tubes for uniform wall temperature conditions in the laminar flow regime. Pure glycerol, water, ethyl alcohol and a water-glycerol mixture were used as working fluids. Brown and Thomas [15] also studied the effect of combined forced and free convection on heat transfer of water in horizontal tubes in the laminar regime. They found that the existing correlations were inaccurate, mostly due to the fact that secondary flow was ignored in previous correlations. Depew and August [16] is another example of an experimental investigation into combined free and forced convection in horizontal tubes with uniform wall temperature in the laminar flow regime using a number of fluids.

Besides the works mentioned briefly, relatively little work has been done on cases with non-uniform heat flux conditions which result in mixed convection scenarios. Such conditions are particularly important to, for instance, linear focusing solar energy heat collectors where applied heat fluxes generally occur on the lower portions of a horizontal tube. For such applications, specifically in low flow rate conditions, it is unclear what effect non-uniform thermal boundary conditions have on the heat transfer coefficient. When heating occurs from below, an enhanced heat transfer coefficient can be expected due to the additional mixing effect caused by the secondary flow, however, the magnitude of the increase in the heat transfer performance is not yet well understood or documented. It is also not clear whether factors such as the angle span of the heat flux, the positioning of the heat flux (symmetric or asymmetric to gravity) and the intensity of the heat flux are important to take into consideration. Little to no experimental work under controlled conditions has been conducted to address this.

The intension of this study is to experimentally determine the effective heat transfer coefficient in a smooth horizontal tube exposed to different circumferential heating distributions. Different heat flux configurations with different angle spans, positions and intensity of the incident heat flux onto a tube were investigated for laminar flow of water.

2. Experimental Setup

2.1 Test Facility

Figure 1 gives a representation of the test facility which consisted of a closed water loop which supplied water at preselected temperatures to an electrically heated test section. Temperature stability was maintained via the use of a 1 000 L storage tank which was thermostatically controlled and connected to a 45 kW chiller unit (item 1). Water was pumped at preselected mass flow rates through the test line (which contained the test section) by means of a positive displacement pump (item 2). Because many of the test case conditions were for mass flow rates that were significantly lower than the rated mass flow rate of the pump, the bypass line was used to maintain smooth flow conditions in the test line by adjusting a hand-operated ball valve (item 7a). Additional hand-operated ball valves (items 7b and 7c) were left open. An accumulator (item 3) was used to further reduce flow pulsations, while a filter (item 4) was used to prevent small particles from entering the test line which might affect the results. Pressure gauges (items 5a-c) were installed to ensure that the pressure in the system could be monitored (pressure readings were not logged since they were not needed during data reduction and falls beyond the scope of this investigation). A Coriolis mass flow meter (item 6) with a measuring range of 0 to 0.604 kg/s and an accuracy of 0.05% of the full range was used to determine the water mass flow rate through the test line. A non-return valve (item 8) was used to isolate sections of the water loop when required. The electrically heated test section (item 9) was connected to a 3 kW direct current power supply (item 10), with voltages and electric current ranges of 0 to 360 V and 0 to 30 A respectively. The accuracy of the power supply was 0.15% for both the voltage and current. Temperature probes on the test section and the mass flow meters were connected to a National Instruments SCXI 1303 32-terminal block fitted to a National Instruments chassis and a desktop computer (item 11). National Instruments LabVIEW software and MATLAB script were used for data acquisition purposes.

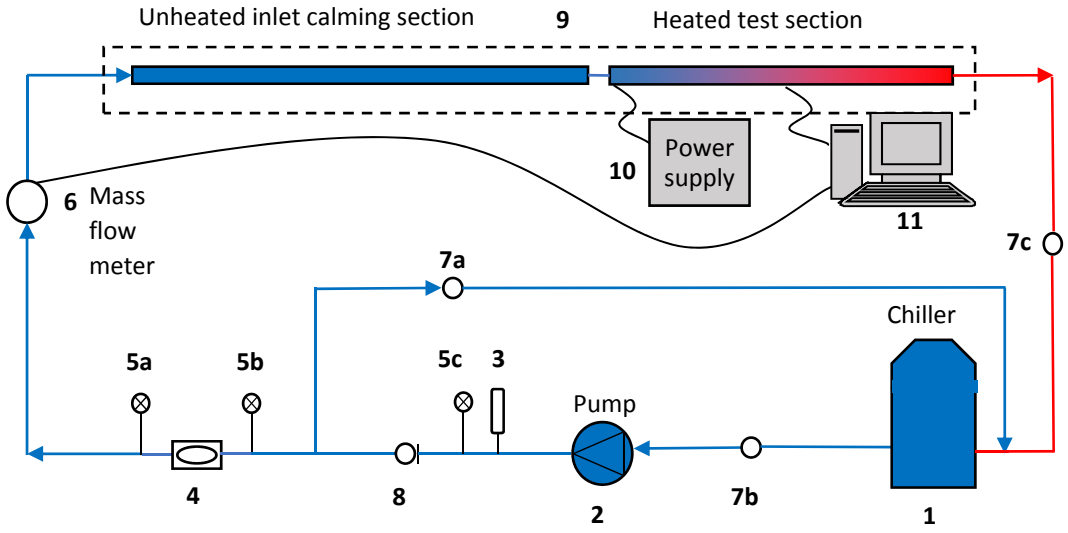

Figure 1 Schematic of experimental facility

2.2 Test Section

Figure 2 shows a schematic side view of the test section. It consisted of a bulk fluid inlet temperature measuring station at m = 0, an unheated (isothermal) inlet calming section, an electric heated section with wall temperature measurement stations, and a bulk fluid outlet temperature measuring station at m = 8.

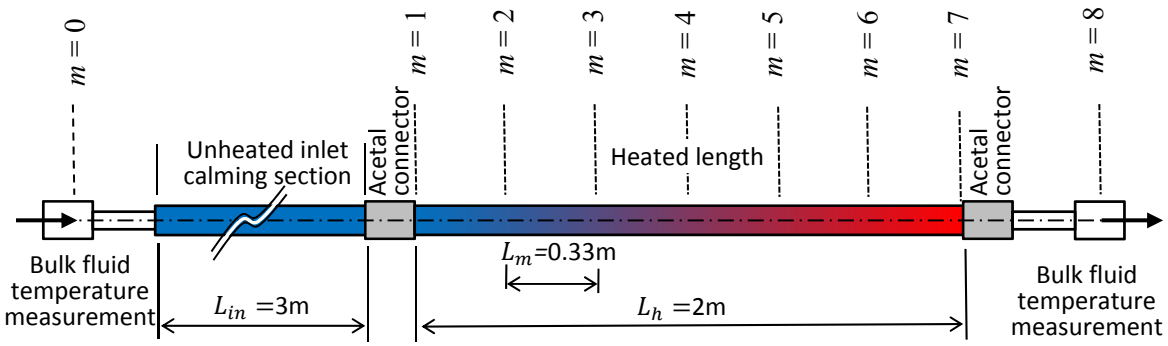

Figure 2: Side view schematic of the test section (not drawn to scale)

At the inlet (m = 0) and outlet (m = 8) the bulk fluid temperatures of the flow were measured by using specially designed measuring stations. Each measuring station was made from a copper tube (due to its high thermal conductivity) and had four T-type thermocouples soldered to the outside at equally spaced positions around the circumference on the downstream end. Special twisted copper inserts

were soldered to the upstream interior of the tubes to disturb the thermal boundary layer. To prevent axial heat conduction to or from the measurement locations, the copper was connected in-line with the rest of the test section and the flow loop circuit by making use of flexible rubber hoses which had a thermal conductivity of 0.19 W/mK. Armaflex type thermal insulation with a thickness of 100 mm and a thermal conductivity of $k_{insul} = 0.036$ W/mK was wrapped around the measuring stations.

After the inlet bulk fluid temperature measurement station, the incoming flow was conditioned and calmed by making use of an isothermal (adiabatic) inlet tube (stainless steel 304). The tube was pre-manufactured via extrusion to produce a seamless passage. It had the same inner diameter (D = 27.8 mm), wall thickness (t = 2.77 mm) and outer diameter (D_o = 33.34 mm) as the heated portion of the test section. Its length (L_{in} = 3 m > $100D$) was selected to provide hydrodynamic developed flow at the start of the heated portion. This was important because the inlet flow velocity distribution profile can have a significant impact on the thermal behaviour in the laminar and transitional flow regimes [17].

The inlet tube section was thermally separated from the heated section by a carefully machined Acetal bush (see Figure 3) with a thermal conductivity of 0.5 W/mK. The bush had an axial length of 130 mm and the same internal diameter as the inlet tube and the heated tube portions. The bush was carefully attached to the tube sections via compression fits. Rubber hoses were secured over either end of the bush to prevent leaks. Care was taken to ensure a smooth internal surface at these joints by enforcing strict manufacturing tolerances of the bush to reduce undesired flow disturbances.

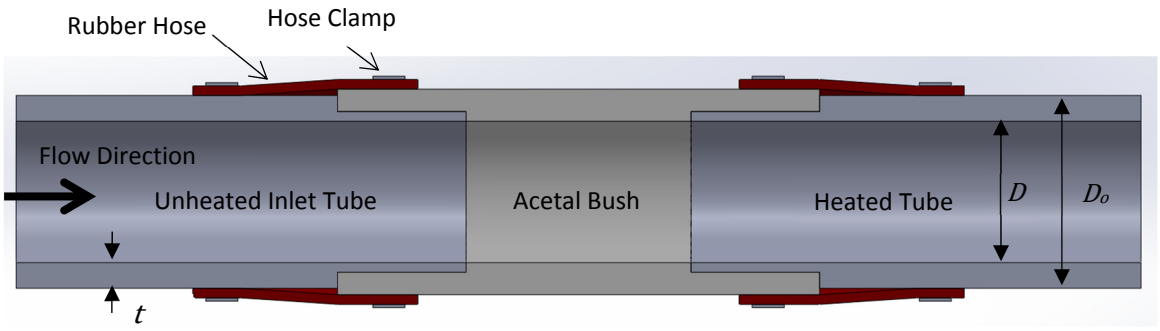

Figure 3: Cross section of the connection between the unheated inlet tube and the heated tube

The heated tube section, which was made of same type of stainless steel tube as the unheated inlet section had a length of 2.000 m (L_h) and was designed to facilitate different heat flux boundary conditions and to enable the measurement of the associated wall temperature profiles. Its specialized design is represented schematically in Figure 4 showing (a) the cross-sectional view down the length

of the tube in the direction of the flow, and (b) a short side-view sectional view perpendicular to the flow.

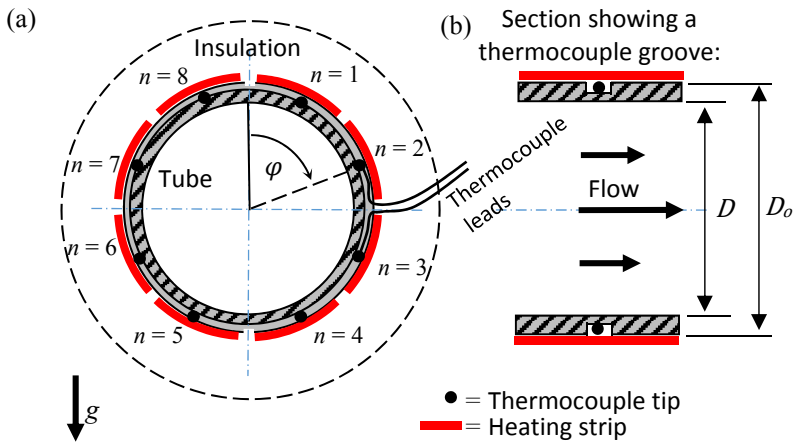

Figure 4: Detailed view of the thermocouple tip and heating element placement (not to scale)

In order to produce different circumferential heat flux conditions, the tube was equipped with 8 heating element strips which were equally spaced around the circumference of the tube and which ran the entire length of the heated portion of the test section. The heating elements are represented in red in the figure and are numbered from n = 1 to n = 8. The angular position of each heated sector will later in the paper be represented with φ defined from top of the tube as is shown in Figure 4. Each heating element consisted of a four-pass constantan heating wire which was directly attached to the outside wall of the tube by means of heat resistant tape to ensure good thermal contact with the tube. The constantan wire had a diameter of 0.38 mm and had extruded PFA electrical insulation to prevent an electric short circuit to the stainless steel tube. The element strips individually had an average resistance of 106.2 Ω, with a maximum variance from the average of 2.2 Ω. This means that all the elements had electrical resistances within 2% of the average resistance. When installed, each element covered an approximate angle span of 45° on the outer surface of the tube and resulted in a 1.8 mm tangential gap between each adjacent heating element strip.

Heating element could be powered individually which enabled the investigation of various heat flux boundary distributions. For this purpose, each element was controlled by a switch and connected to the DC power supply.

Because the main purpose of this study was to investigate the effects of non-uniform heat flux boundary conditions, the boundary conditions applied to the wetted surface needed to be well defined. For this purpose, stainless steel is a suitable tube material due to its relatively low thermal conductivity (k = 16 W/mK) which reduced the tangential and axial heat conduction in the tube wall. This improved the definiteness of the applied boundary conditions.

The heated tube was further also divided into six axial sections, each with an axial length of L_m = 333 mm as is seen in Figure 2. This resulted in the definition of positions m = 1 to m = 7. At locations m = 2 to m = 6, wall temperature measuring stations were created by machining a groove at each location around the circumference of the tube. Each groove housed 8 T-type thermocouples (0.5 mm in diameter) as is shown in Figure 4. Thus, 40 thermocouples were used to obtain the temperature profile around and along the heated tube. Each groove was 1.77 mm deep and 3.2 mm wide. This meant that a wall thickness of approximately 1 mm was left between the inside wall of the tube and the bottom of each groove. The thermocouples were positioned directly below the heating elements and were in contact with the stainless steel surface and were fully contained in the grooves as is shown in the side view of Figure 4. Each tip was held in position by means of Electrolube™ epoxy thermal adhesive with a thermal conductivity of 1.1 W/mK. The thermocouple leads were kept in the groove for a few millimeters before being fed out between the heating element strips. The tube was tightly wrapped with an insulating rubber tape. Hose clamps were also closed around the tube along its length at intervals of 10 mm. This was done to ensure that the heating element strips were securely held in contact with the tube along the entire length and that the thermal contact resistance was relatively uniform along and around the tube.

Both the isothermal inlet length and the heated length were insulated by a 130 mm thick layer of Armaflex™ insulation. The thickness of the insulation resulted in an anticipated maximum heat loss of 3% of the total heat input based on worst case scenario.

3. Experimental Procedure

Before any tests were performed, all measuring devices and probes were calibrated. After installation onto the set-up, the thermocouples were calibrated *in situ* by operating the test bench at a series of isothermal tests at different temperature states (20°C to 53°C using increments of 5°C). A thermostatically controlled electric heated tank was connected to the system and a mass flow rate of 0.2 kg/s resulting in turbulent flow conditions was used for all the calibrating runs. At such a relatively high flow rate sufficient flow mixing occurred which increased the temperature uniformity in the test bench resulting in improved accuracy of the calibration runs. Two PT100 probes that were pre-calibrated to an accuracy of 0.1°C were connected and well insulated at either end of the test section, before and after the measuring stations at m = 0 and m = 8 respectively. For each run, data was recorded once a suitable steady state condition had been met, when the PT100 probe readings remained unchanged for two minutes within a margin of 0.1°C. Second order polynomial calibration curves were used to describe the behavior of each thermocouple which resulted in a calibration accuracy of 0.13°C for all channels.

Table 1 and Figure 5 describe the different test configurations considered in this study. They are organized according to case number (case 1 to 8) with the letter indicating the applied heating rate (A = 800 W, B = 600 W, C = 400 W and D = 300 W). The energized heated arc is defined Figure 5 with red. Table 1 also gives the characteristic angular position of the heated arc in terms of φ as well as the associated local heat flux at the heated arc. Note that φ is measured from the top of the tube to the central point of the heated sector and can only assume a value between 0° (top of tube) and 180° (bottom of tube). Whether heating occurs from the left or the right is treaded the same in terms of the value of φ. For convenience, highlight coloring is used in Table 1 to indicate which test cases shared the same local heat flux. Based on the heated spans and the total energy rate supplied to the heating elements, five local heat flux values ranging from 1658 W/m^2 to 6631 W/m^2 were achieved. The considered heat transfer rates for each angle span and position were determined by the technical limitations of the set-up, the uncertainty analysis ranges of the anticipated results, and lab time constraints.

Table 1: Test cases with heating degrees and corresponding active heating elements

Case number	**Heated span**	Powered heating strips (n)	$\dot{Q}_{tot}$ [W]	$\dot{q}$ [W/m^2]
1A	360°	1 to 8 (all)	800	4421
1B	(φ = not applicable)		600	3316
1C			400	2210
1D			300	1658
2B	Lower 180°	3 to 6	600	6631
2C	(φ = 180°)		400	4421
2D			300	3316
3B	Upper 180°	1,2,7,8	600	6631
3C	(φ = 0°)		400	4421
3D			300	3316
4B	Right 180° (φ = 90°)	1 to 4	600	6631
5B	Left 180° (φ = 90°)	5 to 8	600	6631
6B	Slanted 180°	2 to 5	600	6631
6C	(φ = 135°)		400	4421
7D	Lower 90° (φ = 180°)	4, 5	300	6631
8D	Upper 90° (φ = 0°)	1, 8	300	6631

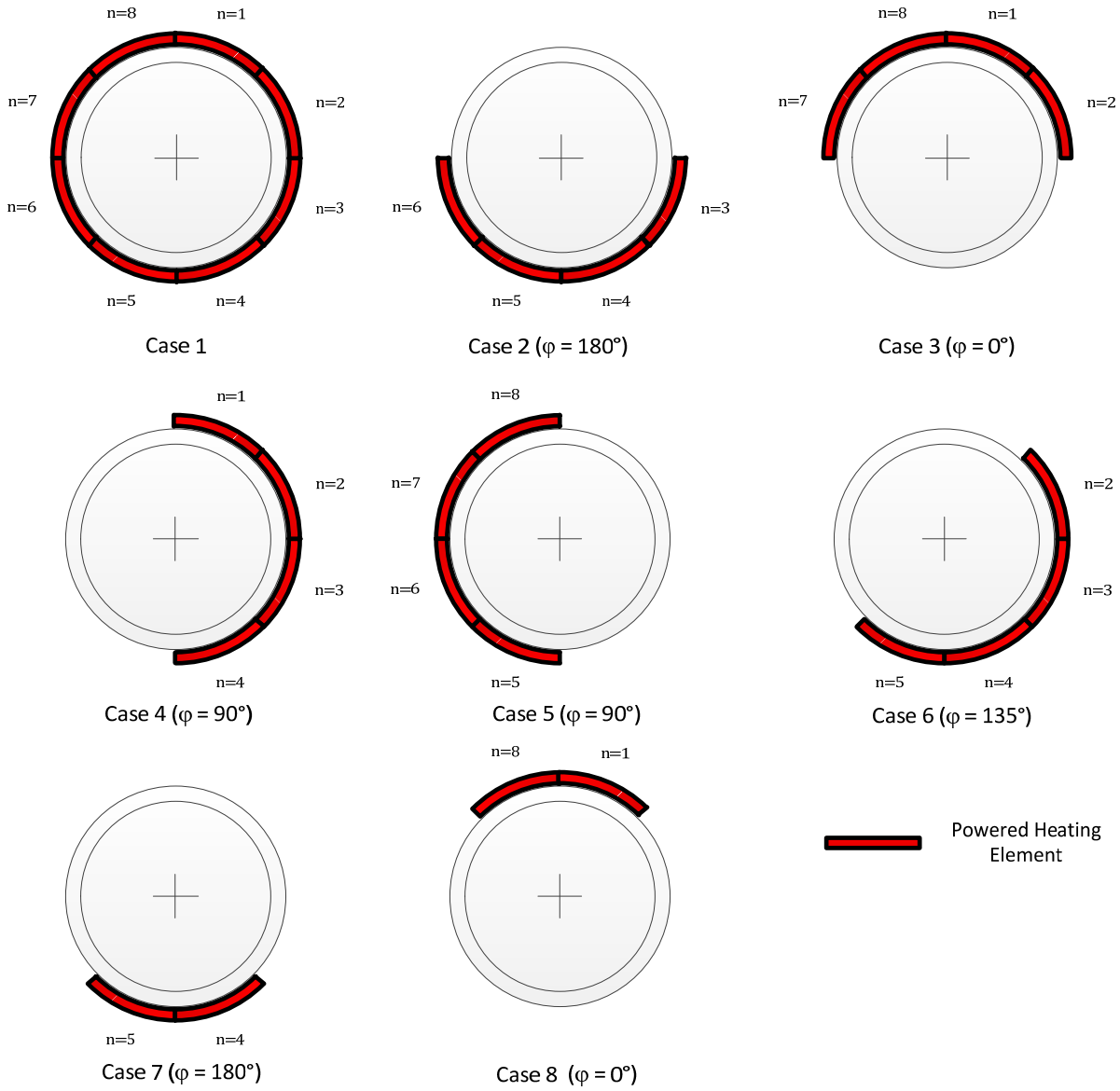

Figure 5: Graphical representation of the test cases

Before each experimental test run, water was circulated through the system at a constant inlet temperature of approximately 20°C. This resulted in average Prandtl numbers in the test section ranging between 6 and 7. The desired heat input was set by selecting the voltage output on the DC power supply and the desired heating elements where powered according to the cases in Table 1. The pump was adjusted in order to achieve the desired mass flow rate. Data from all measuring devices were recorded once steady state conditions were reached when the system temperature and the temperature difference between the inlet and outlet did not fluctuate by more than 0.1°C for one minute. The energy balance was also checked as will be discussed in the next section. For each test point, data was logged at 20 Hz of a period of 10 seconds resulting in 200 data points which were averaged. The test procedure was repeated at different mass flow rates covering Reynolds numbers

from 2600 down to 650 in intervals of approximately 150. As will be shown later, an upper bound Reynolds number of 2 600 was selected for most of the test cases to ensure that all the tests fell in the laminar flow regime.

4. Data Reduction

4.1 Heat Transfer Rates and Energy Balance

The energy balance error was checked by comparing all incoming and outgoing energy rates. The total power input from the power supply was calculated as follows:

$$\dot{Q}_{in} = I_{tot} V_{DC} \tag{1}$$

The voltage (V_{DC}) and current (I_{tot}) were directly logged from the power supply.

The net rate of heat transfer to the water itself, based on the inlet and outlet water states, was calculated as follows:

$$\dot{Q}_{water} = \dot{m} C_p (\overline{T}_{out} - \overline{T}_{in}) \tag{2}$$

The mass flow rate ($\dot{m}$) was obtained from the mass flow meter and the inlet and outlet water temperatures ($\overline{T}_{in}$ and $\overline{T}_{out}$) were obtained using the arithmetic average of the thermocouples at the measuring stations at m = 0 and m = 8 respectively. The specific heat (C_p) was found at the applicable average bulk fluid temperature (determined as the average between the inlet and the outlet temperature) by using the equations of Popiel and Wojtkowiak [18].

The heat loss through the insulation from the heating element to the ambient was calculated as follows:

$$\dot{Q}_{loss} = A_s (T_s - T_{amb}) / R_{insul} \tag{3}$$

The surface area (A_s) was calculated in terms of the length of heated test section (L_h =2 m) and the outer diameter of the insulation (293 mm). The inner surface temperature of the insulation (T_s) was obtained from a thermocouple placed on the inner surface of the insulation and the ambient temperature was obtained from a thermocouple reading taken from the surrounding environment. The thermal resistance of the insulation layer (R_{insul}) was determined as follows:

$$R_{insul} = \frac{r_2}{k_{insul}} ln\left(\frac{r_2}{r_1}\right) \tag{4}$$

The thermal conductivity of the insulation (k_{insul}) was supplied by the manufacturer and the inner and outer radial dimensions of the insulation were measured to be $r_1 = 0.0333$ m and $r_2 = 0.1633$ m.

The following energy balance error expressed in percentage was used by incorporating the heat loss through the insulation:

$$EB = 100 \left| \frac{\dot{Q}_{water} - \left(\dot{Q}_{in} - \dot{Q}_{loss}\right)}{\frac{1}{2}\dot{Q}_{water} + \frac{1}{2}\left(\dot{Q}_{in} - \dot{Q}_{loss}\right)} \right| \quad (5)$$

In this paper the maximum energy balance error is 2.6% with the average error being 1.1%.

4.2 Thermocouple Wall Position Determination

Because the heated stainless steel tube had a relatively low thermal conductivity, the thermocouple readings could not be used directly to represent the wetted wall temperatures. To do this, the temperature difference between the thermocouple tip location and the inner wetted wall was determined by using a semi-numerical/empirical/experimental technique. For this purpose, the radial position of each thermocouple tip had to be determined first. For a particular measuring station m, the thermocouples were not necessarily positioned at the idealized radial position at the bottom of the groove as was initially intended, but in reality, each thermocouple tip probably had a different radial position (depending on the exact groove depth, its exact installed position and its exact size and shape). Such variations would lead to different thermocouples reading different temperatures even if the wetted wall temperature was uniform. Therefore, the impact of possible radial variations had to be calibrated separately for each thermocouple at each measuring station. This was necessary since even though the groove depth within the tube wall was relatively small, a significant temperature difference existed across it in the radial direction.

To find the local thermocouple tip positions, a control volume was drawn around each of the measuring stations as is shown in Figure 6. Positional calibration data was collected experimentally for uniform heated conditions with all the heating elements energized with a total heat input of approximately 800 W. Highly turbulent flow conditions (Re = 10 396) were used such that only forced convection was present ($\mathrm{Ri} = 2.8 \times 10^{-5}$). The turbulent nature of the flow meant that the wetted surface had a circumferentially uniform wall temperature at each axial location for any selected constant radial coordinate in the tube wall. Thus, the relative temperature differences between the thermocouples at n = 1 to n = 8 for a particular station m could be used to determine the different radial thermal resistance variations associated with each thermocouple installation. This was done by making use of the steady state heat conduction equations for a radial system as follows:

$$\dot{Q} = \frac{T_{TC,(m,n)} - \overline{T_{TC,m}}}{R_{TC,(m,n)}} \tag{6}$$

Here $\dot{Q}$ is the local (uniform) radial heat transfer rate as obtained by the heater power rates minus the heat loss rate. $T_{TC,(m,n)}$ is the local thermocouple measurement reading, $\overline{T_{TC,m}}$ is the arithmetic average of the wall thermocouples (n = 1 to 8) at that axial location, and $R_{TC,(m,n)}$ is the thermal resistance between the actual installed radial position of the thermocouple and the average installed radial position at that axial location.

$R_{TC,(m,n)}$ can be expressed as follows:

$$R_{TC,(m,n)} = \frac{\ln\left[\frac{r_{TC,(m,n)}}{\overline{r_{TC,m}}}\right]}{2\pi k L_m} \tag{7}$$

Here $r_{TC,(m,n)}$ is the unknown radial position of an individual thermocouple tip, $\overline{r_{TC,m}}$ is the approximated average radial position at axial position m based on the photographs taken at every thermocouple installation, k is the thermal conductivity of the stainless steel as obtained from the manufacturer and L_m is the distance between two adjacent wall measuring stations.

The individual thermocouple measurements, the average thermocouple measurement at each m location, the assumed average radial distance for each thermocouple as well as the energy rate supplied to each control volume was used to find the actual radial position of each measuring thermocouple by combining equation (6) and equation (7):

$$r_{TC,(m,n)} = \overline{r_{TC,m}} \times e^{\left(2\pi L_m k \frac{T_{TC,(m,n)} - \overline{T_{TC,m}}}{\dot{Q}_m}\right)} \tag{8}$$

Once the actual radial distance for each thermocouple ($r_{TC,(m,n)}$) was calculated, a sensitivity validation check was done against the hypothetically highest and lowest temperature limits associated with thermocouple tips installed respectively in the worst case being flush with the outer tube diameter, and in the best case being perfectly flush with the bottom of the groove. From this it was deduced that all calculated thermocouple positions fell within the plausible radial range.

4.3 Tangential Heat Conduction

For non-uniform heat flux conditions, a numerical model was required to determine the relative tangential heat conduction rates. Heat input from a particular heating element was not necessarily transferred in only the radial direction, but depending on whether the neighboring heating elements were powered or not, a significant proportion of the heat could have been transferred tangentially. This is despite the choice of stainless steel as tube material for its low thermal conductivity. The model

was based on assuming one-dimensional heat transfer in the tangential direction inside the tube wall which has a thickness of t, a thermal conductivity of k, and an assumed uniform hypothetical heat transfer coefficient on the inner surface of h^*. Axial heat conduction was disregarded due to the relatively long distances between the axial measuring stations.

The tube wall was divided into 8 circumferential sectors to match the heating element strip positions. For wall sector n, the energy balance principle can be used to relate the incoming heat transfer rate expressed in terms of the local heating element heat flux ($\dot{q}_{in,n}A_n$) with the heat transfer rate to the bulk fluid temperate, as well as the conductive heat transfer rates to the neighbouring wall sectors $n+1$ and $n-1$. By making use of the combined radial conduction and convection thermal resistance (R_{rad}) and the tangential conduction thermal resistances (R_{n-1} and R_{n+1}), the following steady state equation can be employed to express the local wall temperature (T_n) in terms of an adopted bulk fluid temperature (T_B^*) and the adjacent wall temperatures ($T_{n+1}$and T_{n-1}):

$$\frac{T_{n-1}-T_n}{R_{n-1}}+\frac{T_{n+1}-T_n}{R_{n+1}}+\dot{q}_{in,n}A_n+\frac{T_B^*-T_n}{R_{rad}}=0$$

Where:

$$A_n=\frac{\pi D_{mid}L_m}{8}$$

$$R_{n-1}=R_{n+1}=\frac{\pi D_{mid}}{8ktL_m} \qquad (9)$$

$$R_{rad}=\frac{4t}{k\pi D_{mid}L_m}+\frac{8}{h^*\pi D_{mid}L_m}$$

$$D_{mid}=D+\frac{t}{2}$$

The same can be done for all the sectors resulting in a simple set of 8 linear equations that can be solved for any combination of energized heating elements for an assumed hypothetical internal heat transfer coefficient (h^*)and an assumed bulk fluid temperature (T_B^*). For each possible condition, the percentage of the heat transferred ($\dot{Q}\%$) by each sector to the water in terms of the local applied incoming heat flux from the local energized heating element can be found as follows:

$$\dot{Q}\%=100\frac{\dot{Q}_n}{\dot{Q}_{in,n}} \qquad (10)$$

Where $\dot{Q}_{in,n}$= $\dot{q}_{in,n}A_n$ being the applied heat transfer rate from the external heating element and $\dot{Q}_n = (T_B^* - T_n)/R_{rad}$ being the corrected heat transfer rate on the inner wall for each sector based on the solved set of equations.

This resulted in a numerically obtained database which could be consulted for any energized heating element combination to determine what the effective radial heat transfer rates would be in each of the sectors (n = 1 to n = 8) around the tube. Combined with the calibrated thermocouple radial positions, this allowed for the local wetted wall temperatures to be determined from the measured thermocouple values.

The wetted wall temperature values were obtained at each measuring position based on the previously obtained $r_{TC,(m,n)}$ values:

$$T_{w,(m,n)} = T_{TC,(m,n)} - \dot{Q}_n \frac{\ln\left(\frac{2r_{TC,(m,n)}}{D}\right)}{2\pi k L_m} \tag{11}$$

4.4 Heat Transfer Coefficients

The effective average heat transfer coefficient was found by using the calculated water heat transfer rate, the full internal tube surface area and the temperature difference.

$$\bar{h} = \frac{\dot{Q}_{water} - \dot{Q}_{loss}}{\pi D L_h \Delta\bar{T}_{LMTD}} \tag{12}$$

The average log mean temperature difference between the wall and fluid was calculated using:

$$\Delta\bar{T}_{LMTD} = \frac{\left(\overline{T_{w,m=7}} - T_{B,7}\right) - \left(\overline{T_{w,m=1}} - T_{B,1}\right)}{\ln\left(\frac{\overline{T_{w,m=7}} - T_{B,7}}{\overline{T_{w,m=1}} - T_{B,1}}\right)} \tag{13}$$

The circumferential average wall temperatures $\overline{T_{w,m=1}}$ and $\overline{T_{w,m=7}}$ were found by using a polynomial equation (order 2) fitted to the average wetted wall temperatures between stations m = 2 to m = 6 (each based on the arithmetic average for n = 1 to n = 8).

Due to the fitted insulation and no applied heating between m = 0 and m = 1 and m = 7 and m = 8 the local bulk fluid temperatures, $T_{B,1}$ and $T_{B,7}$ were assumed to be equal to $T_{B,0}$ and $T_{B,8}$ respectively as were measured at m = 0 to m = 8.

The effective Nusselt number was based on the calculated heat transfer coefficient, the inner diameter of the tube and the thermal conductivity of the water (k_{water}) based on the average bulk fluid temperature calculated with the equations of Popiel and Wojtkowiak [18].

$$\overline{\mathrm{Nu}} = \frac{\bar{h}D}{k_{water}} \tag{14}$$

4.5 Other Important Quantities

The Colburn j-factor can be used for an analogy between momentum, mass and heat transfer and can also be used to identify the transition of fluid flow from the laminar to the turbulent regime. It was calculated as follows:

$$j = \frac{\overline{\mathrm{Nu}}}{\mathrm{Re} \times \mathrm{Pr}^{\frac{1}{3}}} \tag{15}$$

The Prandtl number (Pr) was evaluated at the average bulk fluid temperature using the equations of Popiel and Wojtkowiak (1998) [18].

The Reynolds number was calculated as follows:

$$\mathrm{Re} = \frac{\rho V D_i}{\mu} = \frac{4\dot{m}}{\pi \mu D} \tag{16}$$

With the fluid density (ρ) and dynamic viscosity (μ) evaluated at the average bulk fluid temperature using the equations of Popiel and Wojtkowiak (1998) [18].

The Grashof number was calculated in terms of standard gravity (g) the volumetric coefficient of thermal expansion (β) and the kinematic viscosity (ν):

$$\mathrm{Gr} = \frac{g\beta(\overline{T_w} - \overline{T_B})D^3}{\nu^2} \tag{17}$$

β and ν were also evaluated at the average bulk fluid temperature using the equations of Popiel and Wojtkowiak (1998) [18].

The Richardson number was found by dividing the calculated Grashof number by the Reynolds number squared:

$$\mathrm{Ri} = \frac{\mathrm{Gr}}{\mathrm{Re}^2} \tag{18}$$

4.6 Uncertainty and Sensitivity Analysis

The uncertainties for the thermocouples were between 0.1˚C and 0.15˚C, the Coriolis flow meter had an accuracy of 0.05% and the power supply had an accuracy of 0.15% of the nominal value for both

the voltage and current. The uncertainties of the fluid properties, from the equations by Popiel and Wojtkowiak [18],are given in Table 2.

Table 2: Uncertainties of the fluid properties [18]

Property	C_p[J/kgK]	μ[kg/ms]	k[W/mK]	ρ[kg/m³]	**Pr**[-]	β[1/K]
Uncertainty	0.04%	1%	2%	0.004%	2.30%	0.07%

Based on this, the method of Dunn [19] was used to find the uncertainties of the calculated properties as are summarised in Table 3 for low and high Reynolds number conditions, and low and high heat transfer rates. The uncertainty of the Reynolds number value was just above 1%. The average heat transfer coefficient uncertainty was between 2.4% and 2.65% and that of the Nusselt number was between 3.36% and 3.60%.

Table 3: Uncertainties of calculated parameters

Parameter	**Re**	h	$\overline{\mathbf{Nu}}$
Re = 650, $\dot{Q}$ = 300W	1.02%	2.40%	3.36%
Re = 2600, $\dot{Q}$ = 800W	1.03%	2.65%	3.60%

5. Validation and Verification

A number of verifications were performed to determine whether the set-up and the test procedure produced meaningful results.

5.1 Heating element verifications

To ensure that the heating elements individually resulted in the same heat flux on the wetted surface, eight heating test checks were performed, one for each heating element being energised separately. This was done at a Reynolds number of 4700 at a power input of 260 W. The relatively high Reynolds number (when compared to the rest of the cases found in this paper) was chosen to ensure that the system was not in the laminar flow regime. There was a maximum temperature difference of 0.023°C between the highest and the lowest temperature differences (resulting in a maximum difference of 2.5%) which indicated that the relative heating ability of each heating strip was acceptable.

The axial uniformity of heating was also checked. Figure 6 shows the circumferential average wetted wall temperatures along the length of the tube for different mass flow rates with uniform heating. It

can be seen that the wall temperature measurement result appeared as expected and that there was an approximate linear increase in the wall temperature with axial location.

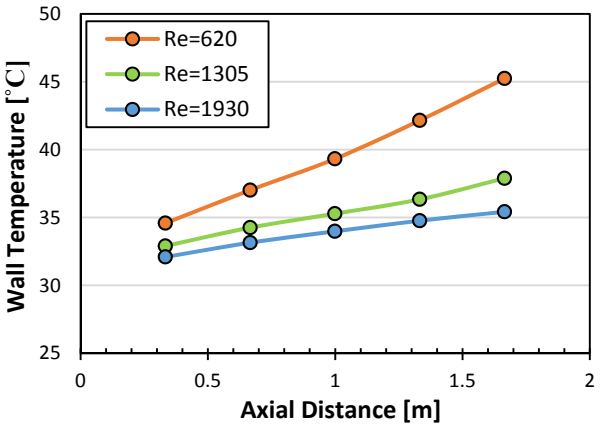

Figure 6: Axial averaged wetted wall temperature profiles for case 1A (uniform heating) at different Reynolds numbers

5.2 Reynolds Number range verification

The onset of the transitional flow regime was determined by conducting experiments over a Reynolds number range from approximately 600 to 4500 at uniform heat flux conditions. For this purpose, case 1B (uniform heat flux with a total heat transfer rate of 600 W) as defined in Table 1 was used. A significant change in the gradient of the j-factors was evident at a Reynolds number of approximately 3000 – 3500. Based on this, the upper bound of the Reynolds number in the test matrix was selected to be 2600 (as mentioned earlier).

5.3 Laminar Comparisons with Correlations from Literature

Experimental data was also compared with correlation predictions from literature which were specifically developed for uniform heat flux. Figure 7 contains the comparison for case 1A (uniform heating with a total heat input of 800 W) for a Reynolds number range of 650 to 1950. Also shown are the uncertainty bars. It can be seen that the experimental Nusselt number are approximately 9.6% higher than the Ghajar and Tam [6] predictions, 41.4% higher that the Morcos and Bergles [4] predictions and 128% higher than the fully developed forced convection Nusselt number of 4.36 (which is only included for relative scaling purposes). It is clear that the differences are greater than the measurement uncertainty. Although the Nusselt numbers obtained in this investigation were higher than the Nusselt numbers predicted by the correlations, some justification for this can be given.

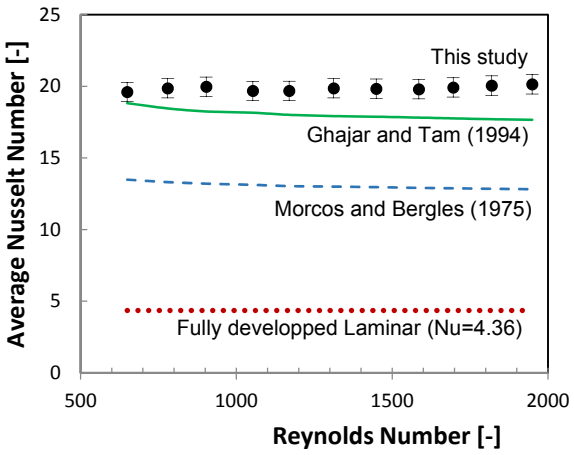

Figure 7: Comparison of laminar data from case 1A to previous works

In the case of Ghajar and Tam, the difference between the experimental data and the predictions of this correlation can be attributed to the mismatch between the Grashof and Prandtl number ranges. The correlation was developed from data with a Grashof range of 1 000 to 2.5 X 10^5 and for a Prandtl number range from 40 to 160 while for the data shown in Figure 8, the Grashof and Prandtl number ranges were 9.95 X 10^7 to 1.29 X 10^8 and 5.48 to 6.46 respectively. The reason for the difference in the predicted Nusselt numbers could be due to the fact that the Ghajar and Tam correlations were not developed with water as the working fluid (Prandtl number range). When considering the Morcos and Bergles correlation, it should be noted that the correlation is for fully developed flow (both hydrodynamically and thermally), while in this investigation the flow is still thermally developing, which is normally associated with higher heat transfer coefficients.

5.4 Turbulent Comparisons with Correlations from Literature

Comparison was also done with literature for the turbulent flow regime as is shown in Figure 8 for data from case 1B for a Reynolds number range of 2600 to 4555. Included in the figure are the correlation predictions of Gnielinski [20], Dittus-Boelter [21], and Sieder-Tate [22]. Relatively good agreement with the Sider-Tate correlation was achieved with an average deviation of 2.53%. When the experimental data was compared to that of the Dittus-Boelter correlation, an average deviation of 19.13% was observed; and for the Gnielinski correlation an average deviation of 11.8% was observed.

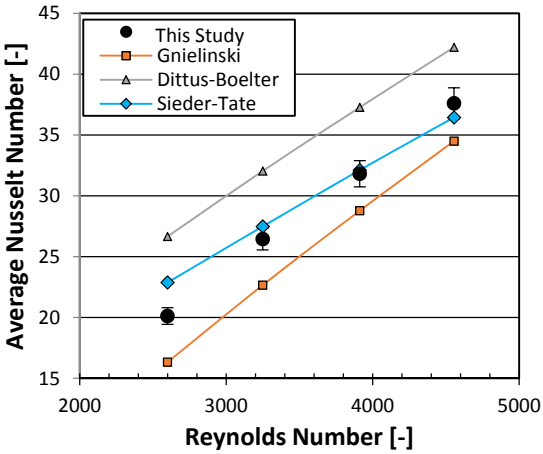

Figure 8: Comparison of turbulent results in case 1B to previous work

6. New Experimental Results

Experimental results are now presented for conditions where buoyancy driven secondary flow plays an important role.

6.1 Wall Temperature Profiles

In this section the circumferential wall temperature distributions are considered for different wall heat flux distributions at two arbitrary selected Reynolds numbers of approximately 650 and 1950. The wall temperature profiles are represented in terms of the difference between the averaged wall temperature (from m = 2 to m = 6) for a particular sector (n = 1 to n = 8) along the length of the heated tube and the average bulk fluid temperature. The reader is reminded that n = 1 and n = 8 are at the top of the tube while n = 4 and n = 5 are at the bottom of the tube.

Figure 9 gives the wall temperature profile for case 1A (uniform heat flux at 800 W and a local heat flux of 4421 W/m^2). It can be seen that the temperature distribution is symmetrical and that warmer wall temperatures were present at the upper region of the tube and colder wall temperature were present at the lower regions of the tube. As expected, higher Reynolds numbers resulted in colder wall temperatures. For Re = 650 the temperature difference was between approximately 9°C and 26°C depending on the circumferential position.

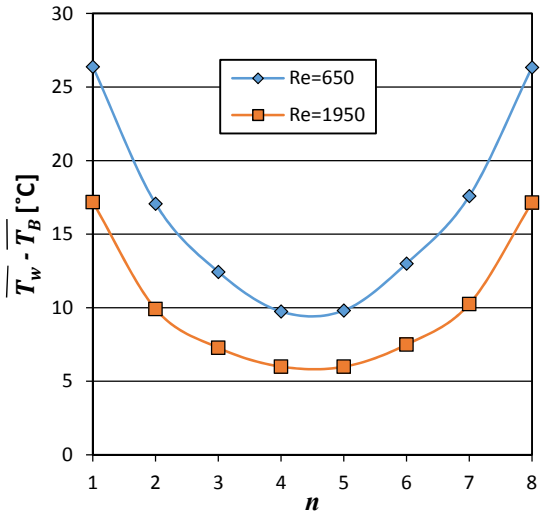

Figure 9: Temperature differences between the wetted wall temperatures and bulk fluid temperatures for case 1A (360˚ heating at 800 W)

Figure 10 shows the temperature profiles for Case 2B with φ =180° (lower 180˚ heating case with 600 W and a local heat flux on 6631 W/m^2). It should be noted that even though the total heat transfer rate is lower than for case 1A, the local heat flux is higher due to the smaller surface area to which it was applied. As before, a symmetric temperature profile was obtained and colder wall temperature were obtained at higher Reynolds numbers. However, in this case the warmer wall temperatures were located at the lower regions of the tube (where heating was applied) and colder wall temperatures were located at the upper region of the tube. It can be noted, however, that much smaller temperature differences existed when compared to the uniform heating case. For Re = 650 it was between approximately 9°C and 16°C, even though this case was operated at higher heat fluxes. The reduction in the temperature differences can be attributed to the effects of buoyancy driven secondary flow which resulted in better fluid mixing and improved convection heat transfer.

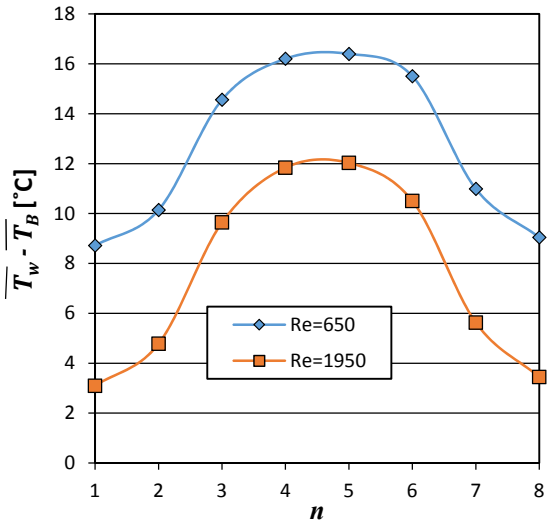

Figure 10: Temperature differences between the wetted wall temperatures and bulk fluid temperatures for case 2B (lower 180° heating at 600 W)

In contrast, Figure 11 shows the temperature profiles for an upper 180° heating case with φ = 0° (case 3B at 600 W and at a local heat flux of 6631 W/m^2). Now, the warmer wall temperatures are located in the upper regions of the tube and the cooler wall temperature at the lower regions of the tube. It should, however, be noted that the wall temperature difference range is significantly higher than before. For Re = 650 this was between approximately 1°C and 40°C. Thus, this case had the highest local wall temperature of all the cases presented thus far. This is an indication of degraded convective heat transfer and can be attributed to the effect of buoyancy driven secondary flow which results in warm fluid being circulated only in the upper regions of the tube. For Re = 1950 it could be noted that a reversed average temperature difference (negative) is present at the lower regions of the tube wall. This indicates that, on average, the lower region of the wall was cooler than the fluid.

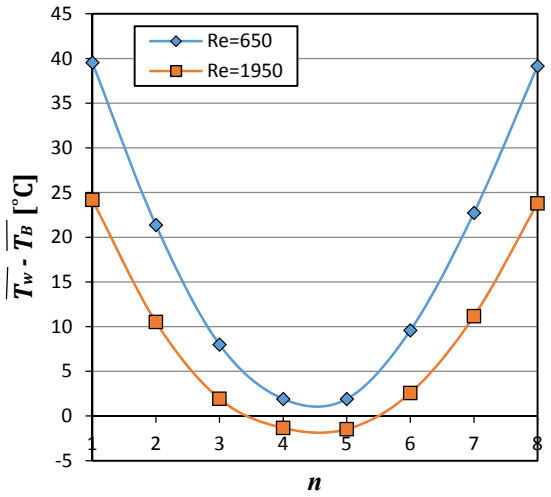

Figure 11: Temperature differences between the wetted wall temperatures and bulk fluid temperatures for case 3B (upper 180˚ heating at 600 W)

Figure 12 and Figure 13 present the temperature profiles for the 180˚ right heating and 180˚ left heating respectively with φ =90° (cases 4B and 5B each at 600 W and a local heat flux of 6631 W/m^2). As expected, it is seen that these profiles mirror each other. Therefore, they may be analyzed together. For Re = 650 the wall temperature difference range was between approximately 5°C and 24°C, which was wider than for the lower 180° heating case at the same heat flux, and narrower than for the upper 180° heating case at the same heat flux. Thus, it could be expected that the effective convective heat transfer coefficient for side heating will be lower than for heating from below, but better than for heating from above. For the side heating cases no heat transfer reversal was noticed at the bottom portion of the tube, but near reversal was present for Re = 1950 on the side opposite from the applied heating span (thus for right hand side heating, near reversal was present on the left hand side and vice versa).

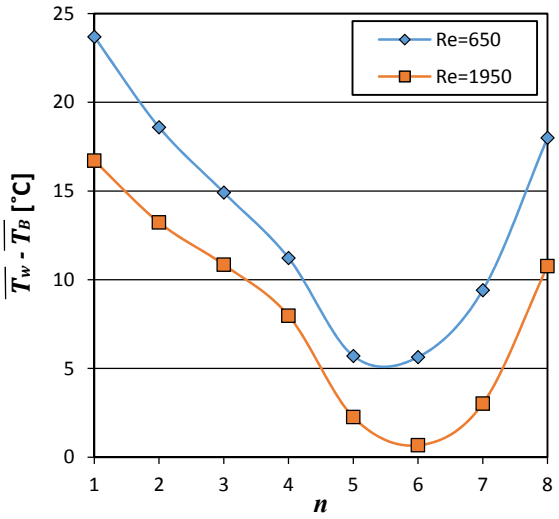

Figure 12: Temperature differences between the wetted wall temperatures and bulk fluid temperatures for case 4B (right 180˚ heating at 600 W)

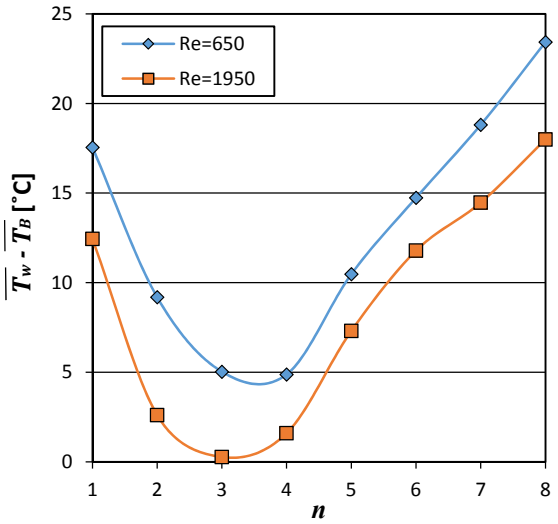

Figure 13: Temperature differences between the wetted wall temperatures and bulk fluid temperatures for case 5B (left 180˚ heating at 600 W)

Figure 14 contains the temperature profiles for slanted 180˚ heating with φ =135° (case 6B at 600 W with a local heat flux of 6631 W/m^2). The non-symmetrical nature of the profiles gives a very clear indication of the buoyancy forces and secondary flow present in the flow being different from some of the previously presented case results. For Re = 650, the wall temperature difference range was between approximately 8°C and 18°C, which was narrower than for the 180° side heating cases, but not as narrow for the lower 180° heating cases (all at the same local heat flux). No heat transfer reversal was present for either Re = 650 or Re = 1950.

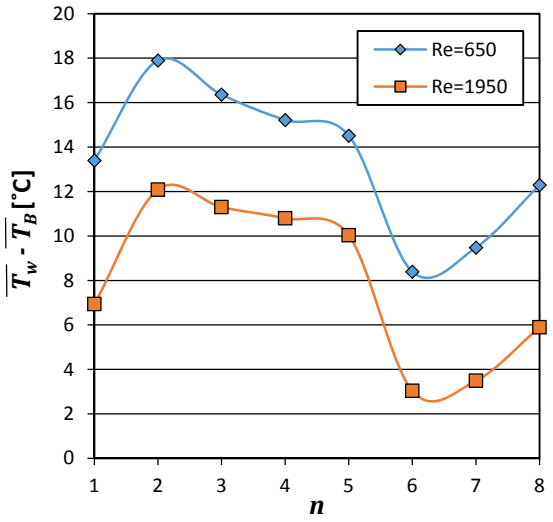

Figure 14: Temperature differences between the wetted wall temperatures and bulk fluid temperatures for case 6B (slanted 180° heating at 600 W)

Figure 15 and Figure 16 are for the lower 90° (with φ =180°) and upper 90° (with φ =0°) heating cases respectively (cases 7D and 8D each at 300 W and a local heat flux of 6631 W/m^2). The obtained temperature profiles are similar in shape to the 180° heating counterpart cases. However, it can be seen that the slopes on the graphs are much more severe in the 90° heating cases. This is to be expected due to the smaller angle span of heating. For Re = 650 the wall temperature difference range was between approximately 2°C and 11°C for lower heating and between approximately -4°C and 18°C for upper heating. Based on this, poorer convective heat transfer is once again expected for the upper heating case. Reversed temperature profiles in the lower regions of the tube were more prevalent than in the case results presented previously. For instance, for case 5D for both Re = 650 and Re = 1950 negative temperature differences were observed at the bottom region indicating that the severe reversal of heat transfer can be expected when a small angle span of heating is applied to the upper region of the tube.

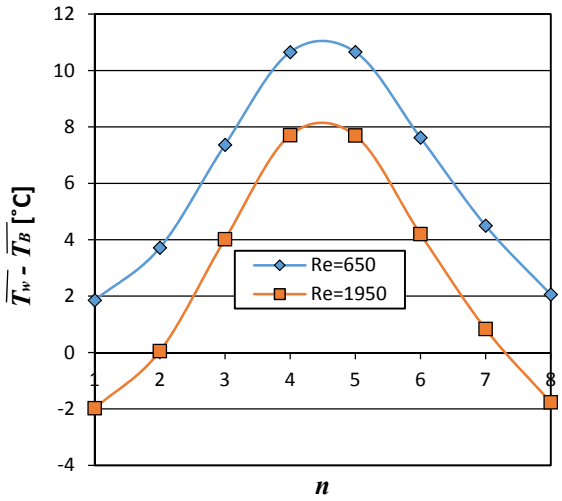

Figure 15: Temperature differences between the wetted wall temperatures and bulk fluid temperatures for case 7D (lower 90˚ heating at 300 W)

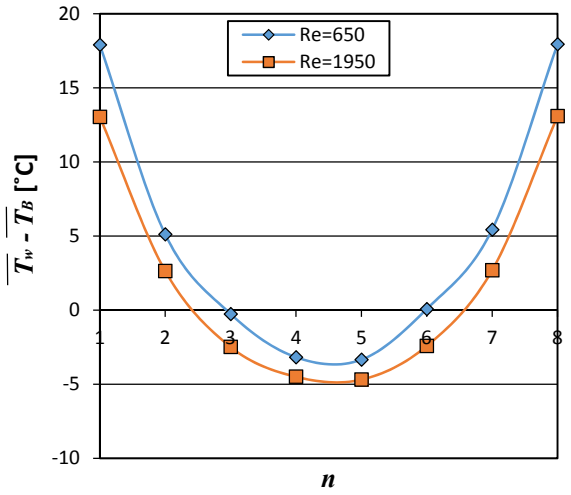

Figure 16: Temperature differences between the wetted wall temperatures and bulk fluid temperatures for case 8D (upper 90˚ heating at 300 W)

6.2 Nusselt number dependence on the heat flux boundary while keeping the local applied heat flux constant

In this section the influence of the applied heat flux distribution on the average Nusselt number is considered for cases which had the same local heat flux. As mentioned earlier, the heat fluxes of interest in this study are 6631 W/m², 4421 W/m² and 3316 W/m². First the Nusselt number results are presented, followed by an analysis of the Richardson number. It should be noted that for a given heat flux, a variation in the angle span of the applied thermal boundary condition resulted in different heat transfer rates to the water. The impact of the heat transfer rate will be considered in the next section.

Figure 17 presents the averaged Nusselt numbers for the 180° heating cases (cases 2B, 3B, 4B/5B and 6B) shown in blue broken lines as well as the two 90° heating cases (cases 7D and 8D) shown in solid red lines, all at the same local heat flux of 6631 W/m². (Uniform 360° results are absent because no uniform heat flux data at that heat flux was available due to the technical limitation of the set-up). It is clear that the heat flux distribution has a very significant influence on the Nusselt number. At a Reynolds number of approximately 650 the difference between the best performing and worst performing cases is 52%, while, for instance at a Reynolds number of approximately 2600, this difference is 21% (using the lower Nusselt number as base of reference). It is seen that although the Nusselt numbers differ greatly at the lower Reynolds numbers, they do tend to converge as the Reynolds number increases. For instance, at Re = 2600, the 180° cases converge to a Nusselt number of approximately 16 to 17, while the 90° cases convergence to a Nusselt number of approximately 14.

Based on the difference between the 180° and 90° cases, it is also clear that the angle span itself is also an important parameter.

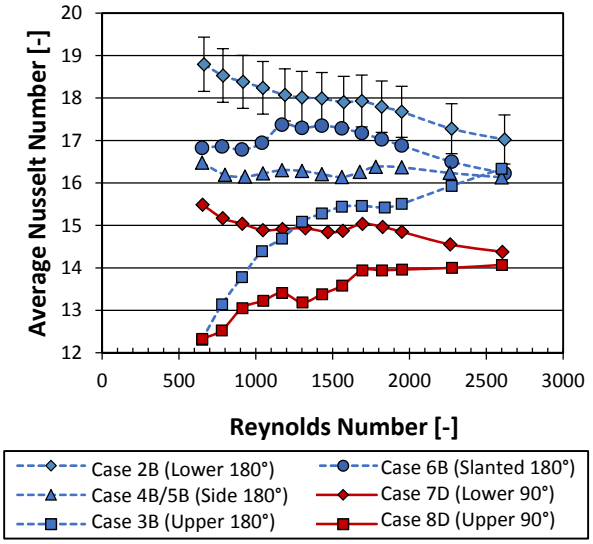

Figure 17: Nusselt numbers for different circumferential heating cases at a local heat flux of 6631 W/m^2

Considering the 180° heating cases, it is clear that the heat flux position has an important impact on the average heat transfer coefficient. Heating on the lower 180° sector (case 2B) with φ =180° exhibited the highest average Nusselt numbers followed by, in decreasing order, slanted heating (case 6B) with φ =135°, side heating (case 4B or 5B) with φ =90° and upper heating (case 3B) with φ =0°. Therefore, in general, the Nusselt number increased when the heated segment on the circumference of the tube was lower down. It can be seen that for cases with φ =180° and with φ =135° (cases 2B and 6B) there was a decrease in the Nusselt number as the Reynolds number increased. For with φ = 90° (case 4B or 5B) no significant change in the Nusselt number in terms of the Reynold number was evident, while for with φ =0° (case 3B) there was an increase in the Nusselt number as the Reynolds number was increased. These variations in the Nusselt number are the result of the increased or decreased strength of the buoyancy driven secondary flow and its relative importance to the forced convection flow component.

Figure 18 shows the Richardson number versus the Reynolds number (on logarithmic-scales) for the cases presented in Figure 17. It can be seen that higher Richardson numbers were present at lower Reynolds numbers and decreased as the Reynolds number increased. Cases 2B, 4B and 6B had similar order of magnitude Richardson numbers, while case 3B (upper 180° heating with φ =0°) had lower Richardson Numbers. In general, the 90° span cases had lower Richardson numbers compared to the 180° span cases, with case 8D (upper 90° heating with φ = 0°) having the lowest Richardson number.

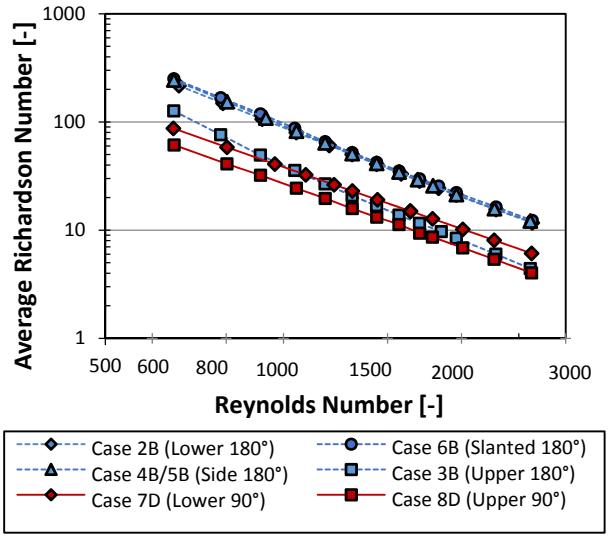

Figure 18: Richardson numbers for different circumferential heating cases at a heat flux of 6 631 W/m²

Similarly, the results for a local heat flux of 4421 W/m² can also be compared with each other. Such a comparison includes the 360° uniform heating case, but excludes the 90° heating span cases (which would have resulted in the measurement uncertainties being too high due to a reduced heat transfer rate in the set up). Figure 19 shows these results for case 1A (360° uniform heating), case 2C (lower 180° heating with φ =180°), case 3C (upper 180° heating with φ =0°) and case 6C (slanted 180° heating with φ =135°). Compared to the 180° span cases, it was found that the 360˚ case produced significantly higher Nusselt numbers, which remained constant at approximately 20 in terms of the Reynolds number. This trend is in agreement with the findings by Okafor *et al.* [11, 12]. As before, the lower 180˚ heating case with φ =180° (case 2C) exhibited higher Nusselt numbers compared to upper heating with φ = 0° (case 3C) and slanted heating with φ =135° (case 6C). The Nusselt number for lower and slanted heating cases reduced as the Reynolds number increased, while the Nusselt number for upper heating increased as the Reynold number increased. This is similar to what was observed previously for a higher heat flux. From Figure 19 it can be seen that the convergence of the Nusselt numbers at higher Reynolds numbers for the 180° heating cases was approximately between 15.5 and 16. This is slightly lower than the anticipated convergence presented earlier in Figure 17 for higher heat flux.

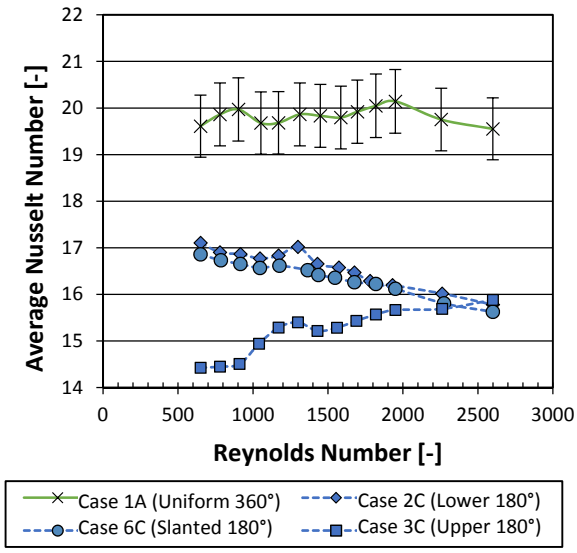

Figure 19: Nusselt numbers for different circumferential heating cases at a local heat flux of 4421 W/m²

Figure 20 shows the average Richardson numbers for the cases plotted in Figure 19. The decreasing trend with Reynolds number is similar as before. Case 1A (uniform 360°) heating exhibited the highest Richardson number, followed by the lower 180° and slanted 180° heating cases (case 2C and 6C). The upper 180° heating case (case 3C) had the lowest Richardson number.

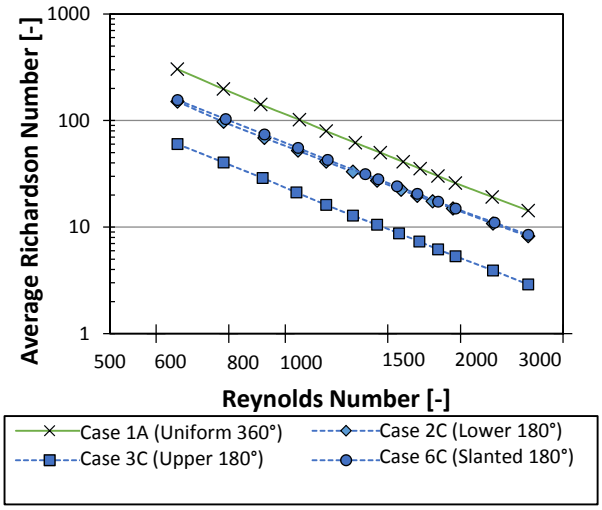

Figure 20: Richardson numbers for different circumferential heating cases at a heat flux of 4421 W/m²

Likewise, the Nusselt number results for a local heat flux of 3316 W/m² can also be compared as is shown in Figure 21. The same trends as in Figure 19 are visible. Uniform 360° heating resulted in a relatively constant Nusselt number of between 19 and 20, while the 180° span heating cases converged at high Reynolds numbers to a value of approximately 15.5. These converged values are

similar to those previously obtained at higher heat fluxes. Similar Richardson number trends were obtained as before and are not repeated here.

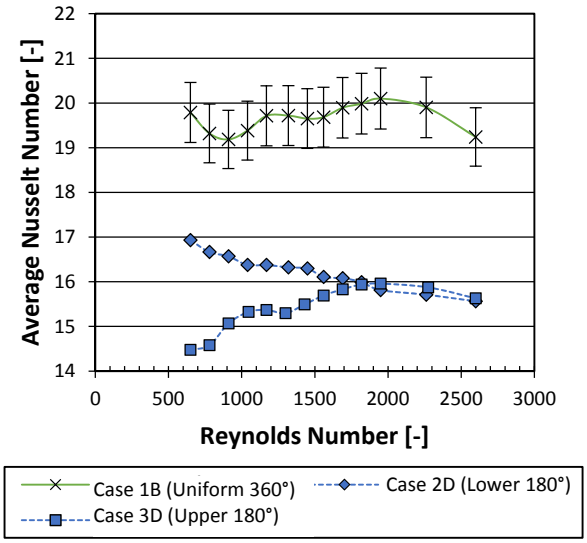

Figure 21: Nusselt numbers vs. Reynolds numbers at a heat flux of 3316 W/m² for different circumferential heating cases

Based on the combined results in Figure 18, Figure 20 it can be deduced that in general the 360° heating cases had higher Richardson numbers compared to the 180° cases, and that the 180° cases had higher Richardson numbers than the 90° cases. This can broadly be used to explain some of the aspects of the combined Nusselt number results presented in Figure 17, Figure 19 and Figure 21. In general, the 360° heating cases had higher Nusselt numbers than the 180° cases, and the 180° cases had higher Nusselt numbers than the 90° cases.

6.3 Influence of the Heating Position

The impact of the heat flux position for a 180° heating span is summarized in terms of φ in Figure 22 for a low Reynolds number, an intermediate Reynolds number and a Reynolds number in the upper region of the laminar flow regime. Judging by the gradients of the Reynolds number profiles, it can be seen that the impact of the heat flux position is more prominent at low Reynolds numbers and less at higher Reynolds numbers. For instance, for Re = 650, heating from below ($\varphi = 180°$) exhibited Nusselt numbers that were 53% higher than for heating from above ($\varphi = 0°$). Nusselt numbers for side and slanted heating ($\varphi = 90°$ and $\varphi = 135°$ respectively) were similar in magnitude and were approximately 34% higher than for heating from above. For Re = 1950 the difference between upper and lower heating was smaller at 14%, and for Re = 2600 the difference was only 4%. This is also a demonstration of the line convergence which is present in Figure 17.

Based on Figure 22, it can also be observed that the Nusselt number increase was not necessarily linear in terms of the angular position. For Re = 650 the dependence is significantly very non-linear, while for Re = 2600 an approximate linear dependence appears to be present.

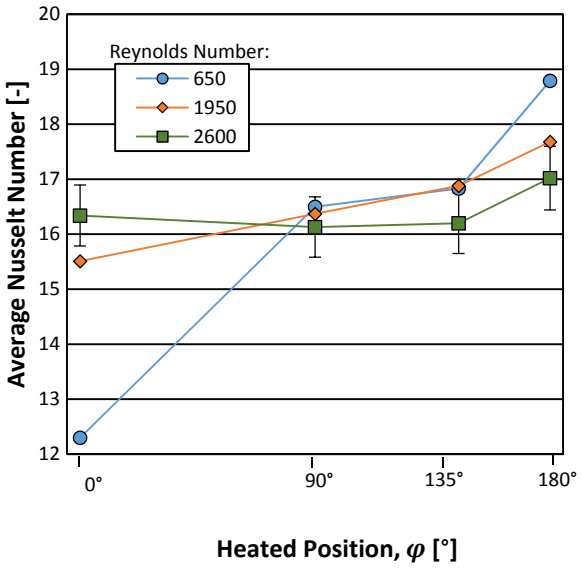

Figure 22: Nusselt number in terms of the position for a 180° heating span at 6631 W/m²

6.4 Influence of the Heat Flux

In this section the impact of the local heat flux intensity on the average Nusselt number is presented. This is done for 360° uniform heating (cases 1A to 1D), lower 180° heating (cases 2B to 2D) and upper 180° heating (cases 3B to 3D).

From Figure 23 it is evident that the Nusselt number is virtually unaffected by a change in heat flux for cases with fully uniform heating. All the data fell approximately within 2.5% of the average value and within the uncertainty band of the measurements. There was however, a significant difference in the Richardson number as is shown in Figure 24. The Richardson numbers increased as the heat flux increased, but did not translate in increased heat transfer coefficients.

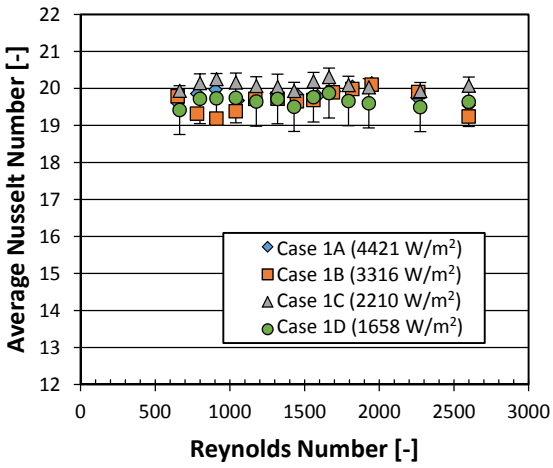

Figure 23: Nusselt numbers for 360˚ uniform heating at different heat flux levels

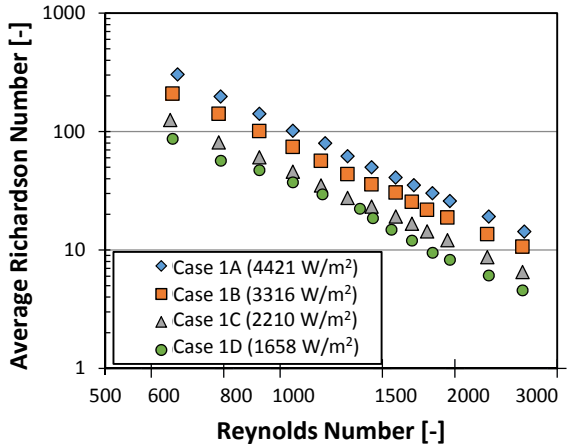

Figure 24: Richardson numbers for 360˚ uniform heating at different heat flux levels

Figure 25 and Figure 26 show the influence of the heat flux intensity for lower and upper 180° heating respectively. For heating from below (Figure 25), it can be seen that increased heat flux resulted in increased Nusselt numbers. At Re = 650, the Nusselt number increased by 13% when the heat flux increased from 3316 W/m^2 to 6631 W/m^2, while at Re = 2600 the Nusselt number increased by 9% for the same heat flux difference. For heating from above (Figure 26) no significant variation in the Nusselt number was present when the heat flux was changed.

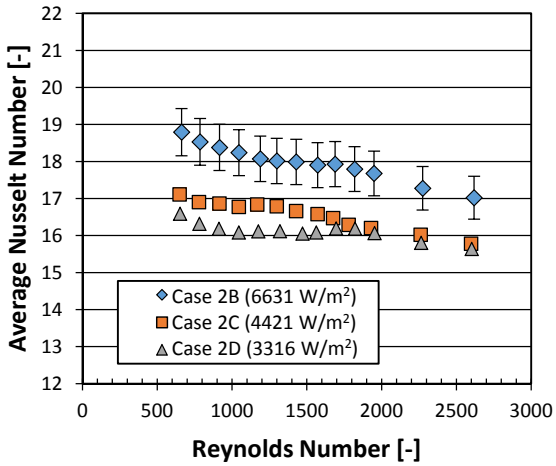

Figure 25: Nusselt numbers vs. Reynolds numbers for lower 180˚ heating cases at different heat flux's

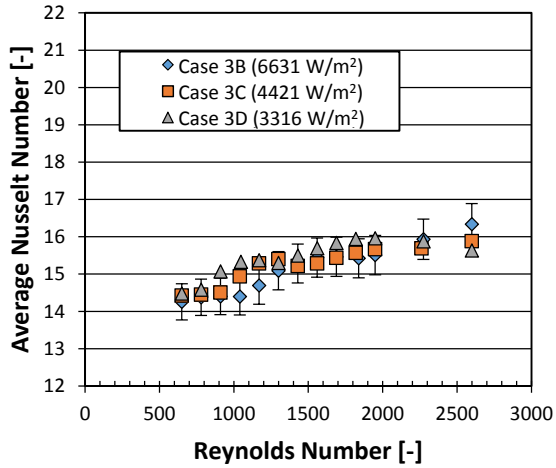

Figure 26: Nusselt numbers vs. Reynolds numbers for upper 180˚ heating cases at different heat flux's

7. Correlations

From the collected data it was shown that the Nusselt number for a uniform heated case was relatively unaffected by the Reynolds number, the Richardson number and the local heat flux. Therefore, a correlation for this case is not proposed in this paper. However, it is evident from the data that for non-uniform heating conditions, the Reynolds number, Richardson number, the local heat flux intensity, the angle span of the applied heating, and the placement of the heating position are important. Thus, correlations are proposed for these cases.

Based on regression techniques the following correlation formulation was found to be suitable to describe all the 180° heating span cases:

$$\mathrm{Nu} = C(\mathrm{Ri} \times \mathrm{Re}^N)^M \, \mathrm{Pr}^P \tag{19}$$

With (for 180° heated spans):

$$C = -0.696 \times [\mathrm{atan}(\varphi - 133.8) - 1.663]$$

$$N = -1.5 \times \cos\varphi$$

$$M = 0.098 \times \left[\mathrm{atan}\left(\frac{\varphi - 134}{23}\right) + 1.364\right]$$

$$P = 1$$

$$0° \leq \varphi \leq 180°$$

The expressions for C, N and M were obtained from the trends of the four heated positions investigated in this study based on a value of P = 1 which suited the data obtained with water.

Figure 27 shows the relationship between the predicted Nusselt numbers and the measured Nusselt numbers for a heating span of 180° for all heat flux values and all angular positions. Good agreement was achieved and 95% of all the data is predicted within 3% of the measured values and 98% of all data is predicted within 5%.

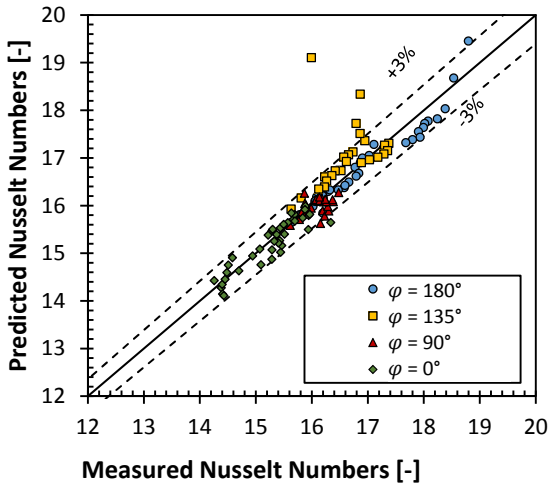

Figure 27: Predicted Nusselt numbers compared to measured Nusselt numbers for a 180° heated span

For convenience, the same correlation format was adopted for the 90° heated span case, but the expressions for C, N and M were based only on the two heated positions investigated in this study and could be updated as more data becomes available in future. For the 90° heated span the Nusselt number can be expressed as follows:

$$\mathrm{Nu} = C(\mathrm{Ri} \times \mathrm{Re}^N)^M \ \mathrm{Pr}^P \tag{20}$$

With (for 90° heated spans):

$$C = -0.565 \times [\mathrm{atan}(\varphi - 140.8) - 1.647]$$

$$N = -1.5 \times \cos\varphi$$

$$M = 0.11 \times \left[\mathrm{atan}\left(\frac{\varphi - 139.3}{22.9}\right) + 1.325\right]$$

$$P = 1$$

$$0° \leq \varphi \leq 180°$$

Good accuracy is obtained with 96% of all the 90° span data being predicted within 3% of the measured data and all of the data being predicted within 5%.

8. Conclusion

Based on the literature review it was found that a need existed to quantify the effect of the intensity and position of non-uniform heat flux distributions on the effective internal heat transfer coefficient, especially in the presence of mixed convection with buoyancy driven secondary flow. An experimental setup to investigate the effect of non-uniform heat flux using water was designed, constructed, verified and validated. The horizontal heated test section tube was constructed from stainless steel, had an inner diameter of 27.8 mm and a length to diameter ratio of 72. The inlet flow was hydrodynamically fully developed. Different heat flux intensities and circumferential distributions where imposed and steady state experimental data was gathered for Reynolds number ranging from 650 to 2600 and local heat flux intensities ranging from 1 658 W/m^2 to 6 631 W/m^2. Heat flux distributions included fully uniform heating, and partial uniform heating with angle spans of 180° and 90°.

It was found that:

- For uniform heating the average Nusselt number was unaffected by the Reynolds number and the heat flux intensity.
- For non-uniform heating the Reynolds number, the heat flux intensity, the heating position and the heating angle span had significant influences on the Nusselt number.
- Larger heating angles spans produced higher Nusselt numbers.
- At low Reynolds Numbers, higher Nusselt numbers were achieved when heating occurred towards the bottom of the tube compared to heating occurring towards the top of the tube.

- For heating which occurred from below, the Nusselt number decreased with an increase in the Reynolds number, while the opposite was true for heating which occurred from above. For lateral heating which occurred from the side, the Nusselt number remained approximately constant with an increase in Reynolds number.
- At high Reynolds numbers the heating position had relatively little impact on the Nusselt number.
- The local heat flux intensity only influenced heating which occurred from below and resulted in increased Nusselt numbers as the heat flux was increased.

Based on the experimental data, two Nusselt number correlations were developed, one each for 180° and 90° angle spans of heating, which took into consideration the influence of the Reynolds number, the Richardson number and the circumferential angular position of the heating. Respectively 95% and 96% of the data is predicted within 3% of the measured data.

9. Acknowledgements and Conflicts of Interest

The funding obtained from the National Research Foundation (NRF), Eskom Tertiary Education Support Programme (TESP), University of Stellenbosch / University of Pretoria, South African National Energy Research Institute (SANERI) / South African National Energy Development Institute (SANEDI), Council for Scientific and Industrial Research (CSIR), Energy Efficiency and Demand Side Management (EEDSM) Hub and NAC is acknowledged and duly appreciated.

On behalf of all authors, the corresponding author states that there is no conflict of interest.

10. References

[1] M. Yasuo, F. Kozo, T. Shinobu, and N. Masakuni, "Forced convective heat transfer in uniformly heated horizontal tubes 1st report—Experimental study on the effect of buoyancy," *International Journal of Heat and Mass Transfer,* vol. 9, pp. 453-463, 1966/05/01 1966.

[2] A. Kupper, E. Hauptmann, and M. Iqbal, "Combined free and forced convection in a horizontal tube under uniform heat flux," *Solar Energy,* vol. 12, pp. 439-446, 1969.

[3] A. Bergles and R. Simonds, "Combined forced and free convection for laminar flow in horizontal tubes with uniform heat flux," *International Journal of Heat and Mass Transfer,* vol. 14, pp. 1989-2000, 1971.

[4] S. Morcos and A. Bergles, "Experimental investigation of combined forced and free laminar convection in horizontal tubes," *Journal of Heat Transfer,* vol. 97, pp. 212-219, 1975.

[5] F. Chou and G. Hwang, "Numerical analysis of the Graetz problem with natural convection in a uniformly heated horizontal tube," *International Journal of Heat and Mass Transfer,* vol. 31, pp. 1299-1308, 1988.

[6] A. J. Ghajar and L.-M. Tam, "Heat transfer measurements and correlations in the transition region for a circular tube with three different inlet configurations," *Experimental thermal and fluid science,* vol. 8, pp. 79-90, 1994/01/01 1994.
[7] H. A. Mohammed and Y. K. Salman, "Experimental investigation of mixed convection heat transfer for thermally developing flow in a horizontal circular cylinder," *Applied thermal engineering,* vol. 27, pp. 1522-1533, 2007.
[8] W. L. Lin and T. F. Lin, "Experimental study of unstable mixed convection of air in a bottom heated horizontal rectangular duct," *International Journal of Heat and Mass Transfer,* vol. 39, pp. 1649-1663, 1996.
[9] A. Elatar and K. Siddiqui, "The effect of mixed convection on the structure of channel flow at low Reynolds numbers," *International Journal of Heat and Fluid Flow,* vol. 46, pp. 29-42, 2014.
[10] C. Chang, X. Li, and Q. Q. Zhang, "Experimental and Numerical Study of the Heat Transfer Characteristics in Solar Thermal Absorber Tubes with Circumferentially Non-uniform Heat Flux," *Energy Procedia,* vol. 49, pp. 305-313, 2014.
[11] I. F. Okafor, J. Dirker, and J. P. Meyer, "Asymmetrical Non-Uniform Heat Flux Distributions For Laminar Flow Heat Transfer With Mixed Convection In a Horizontal Circular Tube," *Heat transfer engineering,* pp. 1-19, 2017.
[12] I. F. Okafor, J. Dirker, and J. P. Meyer, "Influence of non-uniform heat flux distributions on the secondary flow, convective heat transfer and friction factors for a parabolic trough solar collector type absorber tube," *Renewable Energy,* vol. 108, pp. 287-302, 2017/08/01/ 2017.
[13] Z. Huang, Z.-Y. Li, and W.-Q. Tao, *Numerical study on combined natural and forced convection in the fully-developed turbulent region for a horizontal circular tube heated by non-uniform heat flux* vol. 185, 2015.
[14] D. Oliver, "The effect of natural convection on viscous-flow heat transfer in horizontal tubes," *Chemical Engineering Science,* vol. 17, pp. 335-350, 1962.
[15] A. Brown and M. Thomas, "Combined free and forced convection heat transfer for laminar flow in horizontal tubes," *Journal of Mechanical Engineering Science,* vol. 7, pp. 440-448, 1965.
[16] C. A. Depew and S. E. August, "Heat Transfer Due to Combined Free and Forced Convection in a Horizontal and Isothermal Tube," *Journal of Heat Transfer,* vol. 93, pp. 380-384, 1971.
[17] J. Dirker, J. P. Meyer, and D. V. Garach, "Inlet flow effects in micro-channels in the laminar and transitional regimes on single-phase heat transfer coefficients and friction factors," *International Journal of Heat and Mass Transfer,* vol. 77, pp. 612-626, 2014.
[18] C. Popiel and J. Wojtkowiak, "Simple formulas for thermophysical properties of liquid water for heat transfer calculations (from 0 C to 150 C)," *Heat transfer engineering,* vol. 19, pp. 87-101, 1998.
[19] P. F. Dunn, *Measurement and Data Analysis for Engineering and Science, Second Edition*: Taylor & Francis, 2010.
[20] V. Gnielinski, *'G1 Heat Transfer in Pipe Flow' in VDI Heat Atlas*, Second ed. Berlin Heidelberg: Springer-Verlang, 2010.
[21] F. W. Dittus and L. M. K. Boelter, "Heat transfer in automobile radiators of the tubular type," *International Communications in Heat and Mass Transfer,* vol. 12, pp. 3-22, 1985/01/01/ 1985.
[22] E. N. Sieder and G. E. Tate, "Heat Transfer and Pressure Drop of Liquids in Tubes," *Industrial & Engineering Chemistry,* vol. 28, pp. 1429-1435, 1936/12/01 1936.